nature geoscience

ARTICLES

https://doi.org/10.1038/s41561-018-0120-x

An updated stress map of the continental United States reveals heterogeneous intraplate stress

Will Levandowski[1,3]*, Robert B. Herrmann[2], Rich Briggs[1], Oliver Boyd[1] and Ryan Gold[1]

Knowledge of the state of stress in Earth's crust is key to understanding the forces and processes responsible for earthquakes. Historically, low rates of natural seismicity in the central and eastern United States have complicated efforts to understand intraplate stress, but recent improvements in seismic networks and the spread of human-induced seismicity have greatly improved data coverage. Here, we compile a nationwide stress map based on formal inversions of focal mechanisms that challenges the idea that deformation in continental interiors is driven primarily by broad, uniform stress fields derived from distant plate boundaries. Despite plate-boundary compression, extension dominates roughly half of the continent, and second-order forces related to lithospheric structure appear to control extension directions. We also show that the states of stress in several active eastern United States seismic zones differ significantly from those of surrounding areas and that these anomalies cannot be explained by transient processes, suggesting that earthquakes are focused by persistent, locally derived sources of stress. Such spatially variable intraplate stress appears to justify the current, spatially variable estimates of seismic hazard. Future work to quantify sources of stress, stressing-rate magnitudes and their relationship with strain and earthquake rates could allow prospective mapping of intraplate hazard.

Potentially damaging earthquakes occur across the United States and reflect a heterogeneous stress field (Fig. 1). In much of the western United States, rapid strain and abundant seismicity have facilitated detailed quantification of the stress field[1] and its origins[2,3]. By contrast, in situ stress indicators (for example, borehole breakouts) highlight broad patterns in stress directions across the central and eastern United States (CEUS) and Canada[4,5], but low rates of geodetic strain and natural earthquakes[6] have hampered quantification of the full state of stress in a systematic way throughout the region.

In the past several years, however, human activities have increased earthquake rates in the CEUS[7,8], and improved seismic networks have provided high-quality recordings of these and other natural events. We compile 3,848 moment tensors and focal mechanisms (see Methods). Of these, 1,966 are from the CEUS, roughly 7 times as many as the most recent catalogue[9] (although 42 of the latter are average solutions from multiple events and 14 are the results of formal stress inversions), and 100 times as many as early stress maps[1]. We conduct formal stress inversions that quantify the state of stress, principal stress directions and uncertainties more systematically that previously possible.

Observations from focal mechanisms and in situ indicators

Several broad patterns evident in the stress data (Fig. 1a) have previously been documented. In the west, the apparent horizontal maximum compression direction (S_H) remains consistently approximately N–S for more than 1,000 km from the plate boundary, even though contraction transitions to strike-slip and then normal faulting over ~500 km into North America[3]. The progression mirrors analytical solutions[10] that show that the normal stress transmitted from a plate boundary of length L decays by a factor of 10 over a distance of ~0.4 L to 0.8 L into the continent (~1,000 km from the Pacific margin and ~500 km from the Juan de Fuca Plate). Nevertheless, plate-boundary compression cannot cause extension, and eastward asthenospheric flow beneath the west[11] opposes North American plate motion, favouring E–W compression (perpendicular to observed S_H) rather than deviatoric tension in any horizontal direction. Instead, previous work[2,3] has suggested that extension results from elevated lithospheric gravitational potential energy (GPE). The roughly uniform S_H arises because the strain field due to GPE alone is curl-free[12]—similar to a radially extending blob of honey on a flat surface—so superposition of even comparatively small compression from the distant plate boundary controls extension directions[13].

Previous work in the CEUS has also documented a broadly uniform S_H direction (ENE–WSW) and suggested a divide between thrust faulting in southeast Canada and New England and strike-slip faulting in the Midwest[1,4,14]. This difference has been explained as the superposition of a long-wavelength tectonic stress—Mid-Atlantic Ridge push or basal drag—and local perturbations due to postglacial processes, inherited crustal structure or the gravitational effects of a lithospheric keel[4,5,14]. In previous catalogues, the Great Plains were dominated by strike-slip mechanisms from Oklahoma (because of comparatively high historical earthquake rates there; Fig. 1d), prompting interpretations that deformation across the entire CEUS was controlled by plate-boundary compression.

However, new observations reveal several features that are key to understanding the origin of the North American stress field and its variations. First, reverse motion is not confined to northeastern North America but dominates the entire eastern margin. Second, we and others[15] find that Oklahoma is anomalous with respect to its surroundings, and normal faulting, rather than plate-boundary compression, characterizes both the southern[15] and northern Great Plains (Fig. 1a). This pattern can be understood simply, as in the west, as reflecting the waning influence of tectonic stress with distance into North America. (The Mid-Atlantic Ridge system is much longer than either the San Andreas or Cascadian subduction zone, so this transition[10] occurs over thousands rather than hundreds of

[1]USGS, Golden, CO, USA. [2]St Louis University, St Louis, MO, USA. [3]Present address: Colorado College, Colorado Springs, CO, USA.
*e-mail: wlevandowski@coloradocollege.edu

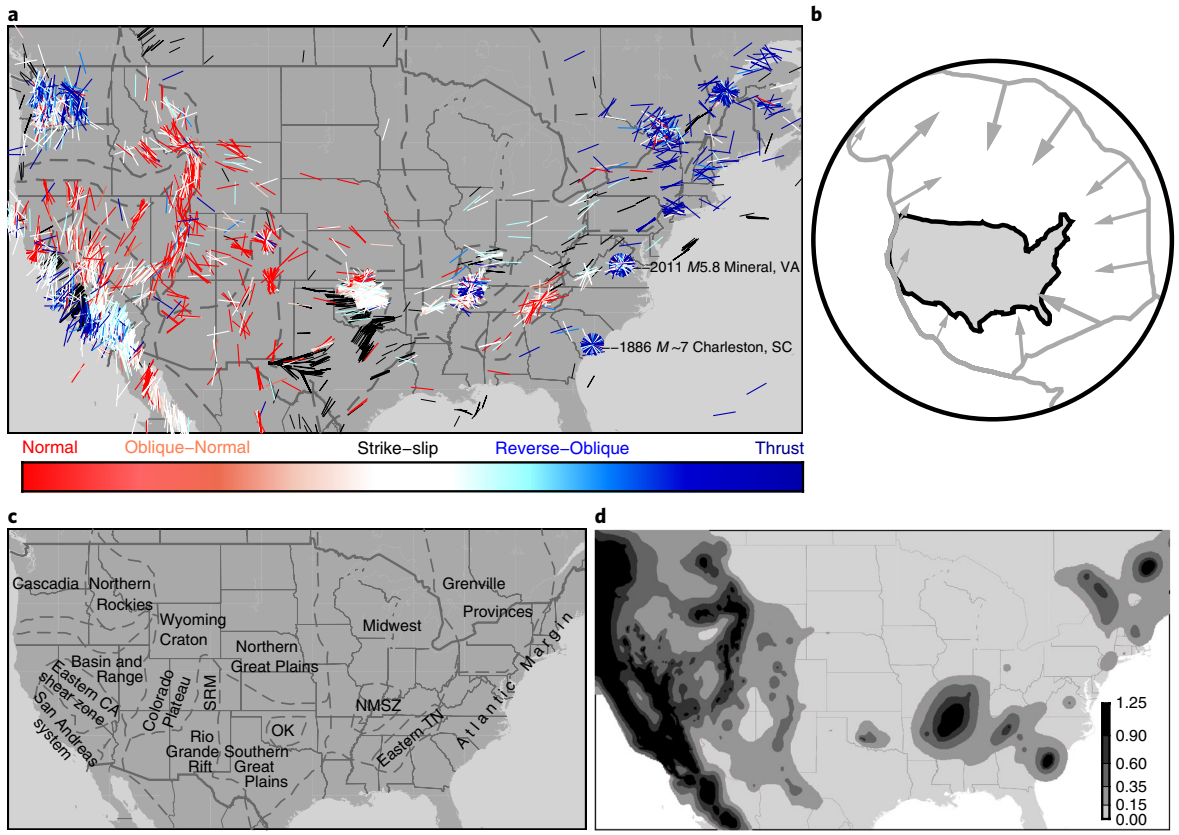

Fig. 1 | Stress indicators and seismic hazard. a, Stress indicators. Coloured bars: focal mechanisms and in situ indicators for which a stress regime is given; oriented parallel to inferred S_H. Black bars: A–C quality in situ indicators[9] averaged over 0.5° bins; lengths reflect data quality. Dashed lines: boundaries of stress provinces in Fig. 2. **b**, Tectonic setting. Schematic diagram of the plate-boundary tractions applied to North America; vector lengths and directions are based on ref. [12]. **c**, Locations discussed in text. SRM, Southern Rocky Mountains. NMSZ, New Madrid seismic zone. **d**, Seismic hazard. The peak ground acceleration expected with a 2% chance in 50 yr (ref. [21]).

kilometres.) Yet, in spite of compressive plate boundaries, a broad region of extension subsumes roughly half of the intraplate United States, stretching from the Basin and Range across the Colorado Plateau and Rockies, and well onto the Plains.

Results and uncertainties from stress inversions

Inversions of focal mechanisms (see Methods) formally quantify the stress field and its variations, lending insight into the processes and forces responsible for deformation. For a set of mechanisms, the best-fitting stress tensor is taken as that which minimizes the angular misfit between the shear traction directions resolved on the fault planes and the slip vectors. That tensor and its uncertainties can be quantified in terms of the maximal horizontal compression direction σ_{Hmax} (distinguished from the direction S_H that is inferred from P axes) and associated style of deformation $A\phi$ (ref. [16]). The latter is a continuum from radial extension at $A\phi = 0$ through normal, strike-slip and reverse faulting to radial contraction at $A\phi = 3$.

Consistent with previous work[1], the stress field of the continental United States can be decomposed into a set of provinces—often, but not always, delineated physiographically—with distinct stress fields, and these provinces vary greatly in size from thousands of kilometres across to as little as 100 km (Fig. 2a). The key features that we will discuss are from these broad provinces (Fig. 2a and Supplementary Figs. 1–3), but increased data density also allows higher-resolution inversions at the scale of individual seismic zones or portions thereof (Fig. 2b), and these inversions confirm that multiple seismic zones within each stress province have statistically similar best-fitting stress tensors. Finally, we perform spatially weighted inversions in each province to illuminate where boundaries between stress regimes are sharp and where they are gradational (Fig. 2c).

Broad consistency in σ_{Hmax} across the CEUS stress provinces suggests that stress directions are controlled by a long-wavelength source, but ENE–WSW σ_{Hmax} accords with either Mid-/North Atlantic Ridge push or basal drag[17,18]. Nevertheless, we resolve a statistically significant difference between σ_{Hmax} along the Atlantic margin (N82 E ± 1°), where it is roughly normal to the Mid-Atlantic Ridge, and in the Grenville terranes of Ontario, Quebec and New York (N57 E ± 2°), where σ_{Hmax} aligns better with North Atlantic Ridge push. The westward decay in $A\phi$ (Fig. 2) across the Atlantic margin (2.63 ± 0.01), Grenville terranes (2.25 ± 0.03), Midwest (1.55 ± 0.04) and southern Great Plains (0.74 ± 0.04) is also more readily explained by waning ridge push, similar to what is expected from analytical solutions[10] and previously suggested for the western United States[2,3].

Extension dominates the west-central United States, but extension directions vary. The approximately N–S σ_{Hmax} in the Cenozoic-active Rockies, Rio Grande Rift, Basin and Range, and Colorado Plateau margins reflects the fact that plate-boundary compression controls the intermediate stress direction even though it is small compared with the maximum (vertical) stress. Similarly, ENE–WSW σ_{Hmax} on the extending southern Great Plains suggests a secondary influence from long-wavelength stress. By contrast, WNW–ESE σ_{Hmax} (N119 E ± 1°) in the nominally stable Colorado Plateau interior, Wyoming Craton and northern Great Plains is distinct from elsewhere in North America and from plate-boundary tractions, suggesting a local source. Moreover, sharp boundaries

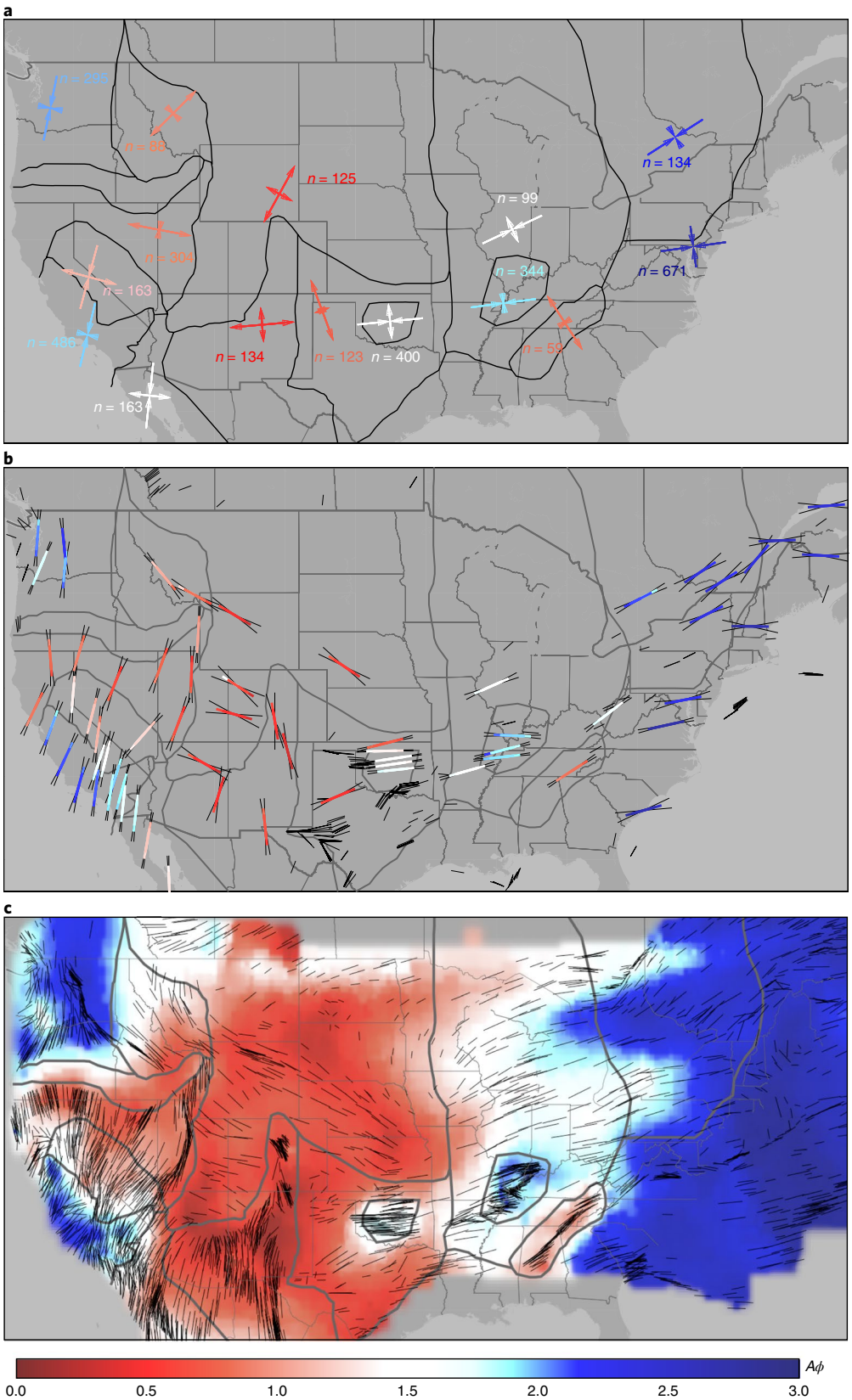

Fig. 2 | Stress inversions. **a**, Inversions in 15 stress provinces. The outward arrows denote horizontal extension, and the inward arrows denote shortening, coloured by $A\phi$. The number of mechanisms in each province is also shown. **b**, Inversions in 62 seismic zones. The bars are oriented parallel to σ_{Hmax}; the thin lines span the 95% confidence interval. Each bar is divided into 5 segments, coloured as the 0.025, 0.16, 0.5, 0.84 and 0.975 quantiles of $A\phi$ (that is, ±2 standard deviation range). The dark black lines are as in Fig. 1a. **c**, Stress map. Dark grey bars: σ_{Hmax} from spatially dependent inversions of focal mechanisms across each province. The lengths are inversely proportional to uncertainty. Background shading: $A\phi$ from spatially dependent inversions across each province.

separate these two provinces and coincide roughly with lithospheric/physiographic boundaries. Small-magnitude horizontal stress variations can alter extension directions, and several causal links between lithospheric structure and secondary stress patterns are possible, including enhanced basal drag in areas of thicker lithosphere[18], GPE gradients[12] and small-scale convection induced by lateral changes in lithospheric thickness[19]. Regardless of what controls extension directions, however, compressional plate-boundary processes alone cannot cause extension in this vast region of the North American interior.

Stress anomalies and seismic hazard in the CEUS. At smaller scales, several modest but statistically significant departures from the broad patterns observed in the CEUS cannot be attributed to plate-boundary processes alone. Strike-slip faulting in central/southern Oklahoma ($A\phi = 1.44 \pm 0.01$) is indeed anomalous with respect to the adjacent southern[15] and northern Plains ($A\phi = 0.74 \pm 0.04$; 0.53 ± 0.04). Reverse-oblique motion in the New Madrid seismic zone is distinct from its surroundings ($A\phi = 1.93 \pm 0.02$ versus 1.55 ± 0.04), and σ_{Hmax} rotates ~20° clockwise (N83 E ± 1° versus N65 E ± 1°)[20]. Finally, Eastern Tennessee and the southern Appalachians host normal faulting ($A\phi = 0.84 \pm 0.07$) that contrasts with thrust to the east and strike-slip to the west.

Each of these anomalous zones also hosts elevated historical/prehistorical earthquake rates, and they are consequently mapped[21] as three of the four highest-hazard natural seismic zones in the CEUS (Fig. 1d). Understanding what connections, if any, exist between the anomalous stress states and localized deformation is critical. Three competing classes of hypotheses have been proposed to explain focused Quaternary seismicity, with differing implications for the relationships among past earthquakes, future hazard and long-term stress and strain, however.

Transient stress perturbations—such as from erosion/deposition or deglaciation[22]—of as little as ~0.5 MPa (ref. [23]) can trigger slip, so intraplate seismicity need not be stationary over time, possibly making past earthquakes a poor proxy for future hazard[6]. The differential stress required for earthquake nucleation is ~100 times these minor fluctuations, however, so they alone cannot explain the observed stress anomalies. By contrast, major earthquakes create larger-magnitude stress changes, so aftershocks near the fault can illuminate spatially variable stress. For example, following the 2002 *M*7.9 Denali, AK, earthquake, perturbations to σ_{Hmax} could be observed within ~10 km of the fault plane, but no significant deviation in $A\phi$ was observed[24], and within 5 km of the 2011 *M*5.8 Mineral, VA, and 1886 $M \sim 7$ Charleston, SC, epicentres (both reverse-faulting events; locations on Fig. 1a), we indeed find that σ_{Hmax} orients radially to the epicentre (Supplementary Fig. 5). In New Madrid, Eastern Tennessee and central/southern Oklahoma, however, stress is consistent—and consistently different from adjacent areas—over scales of hundreds of kilometres (Fig. 2 and Supplementary Fig. 5), and these differences are primarily in $A\phi$. Therefore, even if transient processes influence earthquake rates[6,22,25], they cannot explain the anomalous stress observed.

Weak regions—either frictionally weak crust or low-viscosity ductile material—elevate long-term earthquake rates[26]. Early studies discerned no difference in stress between seismic zones and adjacent areas and consequently suggested that intraplate strain localizes in weak crust[1]. Subsequent work, however, revealed that nearly all CEUS earthquakes are compatible with fault frictions similar to laboratory measurements (about 0.6–0.8) and near-hydrostatic pore-fluid pressures[4,14]. We also find that systematic differences in fault friction and pore pressure cannot account for the anomalies observed in Eastern Tennessee, New Madrid and central/southern Oklahoma (Supplementary Fig. 4 and Supplementary Table 1). Low-viscosity lower crust or upper mantle strains proportionally faster under a given stress, requiring proportionally greater earthquake rates in the overlying crust[27]. Nevertheless, the viscous strain rate tensor is proportional to the stress tensor (in isotropic media), so low-viscosity zones do not explain changes in the style of faulting without progressive decoupling of the brittle and ductile portions of the lithosphere with time[27]. Additional work considering the effects of rheology and mechanical anisotropy on faulting styles in these three zones is needed.

Persistent stress perturbations—which are superposed on (that is, the tensor sum with) the regional, long-term loading—could both elevate long-term earthquake rates and locally alter stress. To substantially alter stress orientation and/or faulting style at fault-zone scales, such perturbations must have similar lateral extents to the stress anomalies (~100 km and greater) and magnitudes similar to or greater than that of the regional long-term fault loading[28]. Laterally variable asthenospheric flow[19,29] and the density distribution within the lithosphere[2,3,30–32] are possible sources of localized stress. Importantly, where perturbations sum constructively with the regional field and increase net deviatoric loading, they will not only alter $A\phi$ and/or σ_{Hmax} but also increase long-term strain and therefore earthquake rates[13,32], offering a unified explanation for focused seismicity and anomalous stress.

Some convection models predict convergent asthenospheric flow and downwelling beneath New Madrid, which would favour E–W compression[29]; a similar pattern beneath Oklahoma and focused upwelling beneath the southern Appalachians could explain the anomalous styles of faulting observed. Some tomograms depict modestly slow upper mantle—inferred to be warm and buoyant—beneath the southern Appalachians[33], but a larger-magnitude low-velocity zone beneath New Madrid[33] and the lack of any anomaly beneath Oklahoma[34] cast doubt on the role of upper mantle convection in producing the anomalous faulting styles observed.

Alternatively, density anomalies inherited from prior tectonic events can influence modern deformation. Indeed, each of the three seismic zones in question is the site of repeated previous tectonism and pervasive crustal modification. Dense lower crust beneath New Madrid[31,32] and in other failed rifts[30]—such as the Oklahoma Aulacogen—locally promotes rift-normal contraction. By contrast, lower crustal delamination or serpentinization has been proposed in Eastern Tennessee and the southernmost Appalachians[35]; such an increase in crustal buoyancy would locally induce uplift and favour horizontal extension in the overlying material[36].

Regardless of the origin of these anomalies, it is clear that the intraplate stress field is variable, with long-wavelength variations overprinted by more local and subtle changes to style, orientation and earthquake rate. Stress variations may focus intracontinental earthquakes, so the current, spatially heterogeneous view of CEUS seismic hazard[21] appears warranted. More precise quantification of sources of stress and their relationship with strain and earthquake rates will aid in prospective mapping of intraplate seismic hazard.

Methods

Methods, including statements of data availability and any associated accession codes and references, are available at https://doi.org/10.1038/s41561-018-0120-x.

Received: 5 January 2018; Accepted: 9 April 2018;
Published online: 21 May 2018

References

1. Zoback, M. L. & Zoback, M. D. State of stress in the conterminous United States. *J. Geophys. Res.* **85**, 6113–6156 (1980).
2. Jones, C. H., Unruh, J. R. & Sonder, L. J. The role of gravitational potential energy in active deformation in the southwestern United States. *Nature* **381**, 37–41 (1996).
3. Flesch, L. M., Holt, W. E., Haines, A. J. & Shen-Tu, B. Dynamics of the Pacific–North American plate boundary in the western United States. *Science* **287**, 834–836 (2000).

4. Zoback, M. L. Stress field constraints on intraplate seismicity in eastern North America. *J. Geophys. Res.* **97**, 11761–11782 (1992).
5. Reiter, K. et al. A revised crustal stress orientation database for Canada. *Tectonophysics* **636**, 111–124 (2014).
6. Stein, S. & Liu, M. Long aftershock sequences within continents and implications for earthquake hazard assessment. *Nature* **462**, 87–89 (2009).
7. Ellsworth, W. L. Injection-induced earthquakes. *Science* **341**, 1225942 (2013).
8. Weingarten, M. et al. High-rate injection is associate with the increase in U.S. midcontinent seismicity. *Science* **348**, 1336–1340 (2015).
9. Heidbach et al. *World Stress Map Database 2016* (GFZ, 2016); https://doi.org/10.5880/WSM.2016.001
10. England, P., Houseman, G. & Sonder, L. J. Lengthscales for continental deformation in convergent, divergent and strike-slip environments. *J. Geophys. Res.* **90**, 3551–3557 (1985).
11. Silver, P. G. & Holt, W. E. The mantle flow field beneath western North America. *Science* **295**, 1054–1057 (2002).
12. Humphreys, E. D. & Coblentz, D. North American dynamics and western U.S. tectonics. *Rev. Geophys.* **45**, RG3001 (2007).
13. Ghosh, A. & Holt, W. E. Plate motions and stresses from global dynamic models. *Science* **335**, 838–843 (2012).
14. Hurd, O. & Zoback, M. D. Intraplate earthquakes, regional stress, and fault mechanics in the central and eastern U.S. and southeastern Canada. *Tectonophysics* **581**, 182–192 (2012).
15. Lund-Snee, J. E. & Zoback, M. D. State of stress in Texas: implications for induced seismicity. *Geophys. Res. Lett.* **43**, 10208–10214 (2016).
16. Simpson, R. W. Quantifying Anderson's fault types. *J. Geophys. Res.* **102**, 17909–17919 (1997).
17. Zoback, M. L. & Zoback, M. D. Tectonic stress field of the continental United States. *GSA Memoir* **172**, 523–540 (1989).
18. Gough, D. I., Fordjor, C. K. & Bell, J. S. A stress province boundary and tractions on the North American plate. *Nature* **305**, 619–621 (1983).
19. Becker, T. W. et al. Western US intermountain seismicity caused by changes in upper mantle flow. *Nature* **524**, 458–461 (2015).
20. Hurd, O. & Zoback, M. D. Regional stress orientations and slip compatibility of focal mechanisms in the New Madrid Seismic Zone. *Seismol. Res. Lett.* **83**, 672–679 (2012).
21. Petersen, M.D. et al. *Documentation of the 2014 Update of the United States National Seismic Hazard Maps* USGS Open File Report 1091 (USGS, 2014).
22. Calais, E. et al. Triggering of New Madrid seismicity by late-Pleistocene erosion. *Nature* **466**, 608–611 (2010).
23. Stein, R. The role of stress transfer in earthquake occurrence. *Nature* **402**, 605–609 (1999).
24. Wesson, R. L. & Boyd, O. S. Stress before and after the 2002 Denali Fault earthquake. *Geophys. Res. Lett.* **34**, L07303 (2007).
25. Mueller, K., Hough, S. E. & Bilham, R. Analysing the 1811–1812 New Madrid earthquakes with recent instrumentally recorded aftershocks. *Nature* **429**, 284–287 (2004).
26. Lowry, A. R. & Pérez-Gussinyé, M. The role of crustal quartz in controlling Cordilleran deformation. *Nature* **471**, 353–357 (2011).
27. Zoback, M. D. & Townend, J. Implications of hydrostatic pore pressures and high crustal strength for the deformation of continental lithosphere. *Tectonophysics* **336**, 19–30 (2001).
28. Sonder, L. J. Effects of density contrasts on the orientation of stresses in the lithosphere: relation to principal stress directions in the Transverse Ranges, California. *Tectonics* **9**, 761–771 (1990).
29. Forte, A. M. et al. Descent of the ancient Farallon slab drives localized mantle flow beneath the New Madrid seismic zone. *Geophys. Res. Lett.* **34**, L04308 (2007).
30. Zoback, M. L. & Richardson, R. M. Stress perturbation associated with the Amazonas and other ancient rifts. *J. Geophys. Res.* **101**, 5459–5475 (1996).
31. Grana, J. P. & Richardson, R. M. Tectonic stress within the New Madrid seismic zone. *J. Geophys. Res.* **101**, 5445–5458 (1996).
32. Levandowski, W., Boyd, O. S. & Ramirez-Guzmán, L. Dense lower crust elevates long-term earthquake rates in the New Madrid seismic zone. *Geophys. Res. Lett.* **43**, 8499–8510 (2016).
33. Biryol, C. B. et al. Relationship between observed upper mantle structure and recent tectonic activity across the southeastern United States. *J. Geophys. Res.* **121**, 3393–3414 (2016).
34. Shen, W. & Ritzwoller, M. H. Crustal and uppermost mantle structure beneath the United States. *J. Geophys. Res.* **121**, 4306–4342 (2016).
35. Graw, J. H., Powell, C. A. & Langston, C. A. Crustal and upper mantle velocity structure in the vicinity of the Eastern Tennessee seismic zone based upon radial P-wave transfer functions. *J. Geophys. Res.* **120**, 243–258 (2015).
36. Cooley, M. T. *A New Set of Focal Mechanisms and a Geodynamic Model for the Eastern Tennessee Seismic Zone*. MSc thesis, Univ. Memphis (2014).

Acknowledgements

J. Hardebeck, M. Zoback and M. L. Zoback provided helpful comments and discussions during preparation of this manuscript. W.L. was funded by the USGS Mendenhall Postdoctoral Fellowship and Earthquake Hazards Program.

Author contributions

W.L. managed catalogue compilation, stress inversions, figure generation and manuscript preparation. R.B.H. generated a plurality of the focal mechanisms and aided in the uncertainty analysis for individual data. All authors collaborated on figure generation, drafting and hypothesis testing.

Competing interests

The authors declare no competing interests.

Additional information

Supplementary information is available for this paper at https://doi.org/10.1038/s41561-018-0120-x.

Reprints and permissions information is available at www.nature.com/reprints.

Correspondence and requests for materials should be addressed to W.L.

Publisher's note: Springer Nature remains neutral with regard to jurisdictional claims in published maps and institutional affiliations.

Methods

Inversions of coseismic slip data. Inversions of fault slip data such as focal mechanisms are well established and generally stem from the axiom that the coseismic slip vector parallels the shear traction resolved on the fault plane[37,38]. This direction depends linearly on the normalized stress tensor, which can be fully described by the orientations of the three mutually orthogonal principal stresses and the stress ratio ϕ:

$$\phi = \frac{\sigma_2 - \sigma_3}{\sigma_1 - \sigma_3} \quad (1)$$

In equation (1), σ_1, σ_2 and σ_3 are the maximally compressive, intermediate and minimally compressive principal stresses, respectively. With multiple observations that occur in response to the same state of stress, this linear system becomes overdetermined and thus suitable for formal inversion for the best-fitting tensor for those observations. As such, there is no assumption made about the relationship between P/B/T axes and stress directions. For this reason, we draw a distinction between the stress directions inferred solely from P/T/B axes, which we called $S_{1,2,3}$, and the results of inversions, which we call $\sigma_{1,2,3}$.

The style of faulting (that is, normal, strike-slip or reverse) and ϕ define the seismotectonic setting $A\phi$ (ref. [16]):

$$A\phi = (n + 0.5) + (-1)^n(\phi - 0.5) \quad (2)$$

Following ref. [4], n is 0 for normal faulting, 1 for strike-slip and 2 for thrust. For example, in a thrust-faulting regime, as ϕ approaches 0 (that is, $\sigma_2 \approx \sigma_3$), $A\phi$ approaches 2. Similarly, a strike-slip regime with ϕ approaching 1 also has $A\phi$ approaching 2. These states of stress are identical since $\sigma_{Hmax} > \sigma_{Hmin} \approx \sigma_{vertical}$, and favour oblique contraction. Thus, each inversion derives a quantitative estimate of the best-fitting seismotectonic setting ($A\phi$) and principal stress directions.

To assess uncertainty, we conduct 5,000 realizations of the inversion for each stress province and each seismic zone (using code modified from ref. [39]). Each realization jackknife-resamples, removing $\sqrt{n}$ mechanisms, where n is the total number in the zone/province. To account for uncertainty in individual mechanisms, we add ±15° of noise to each mechanism in each realization, which—as discussed more fully in the section entitled `Uncertainty of individual mechanisms', below—approximates the 95% confidence interval of most of the mechanisms in our catalogue. Since there is ambiguity in which of the nodal planes is the focal plane and which is the auxiliary plane, each inversion[39] begins by randomly choosing which nodal plane is the focal plane for each event. It then inverts the attendant slip vectors for the optimal stress tensor (that is, the normalized tensor that minimizes angular misfit between the shear traction on the putative focal planes and the slip vectors). Iteratively, it then revisits each event, calculates the instability factor of the two nodal planes, selects the plane with the greater instability factor in the currently estimated stress field and then inverts the group of mechanisms again. Only a few (generally 1 to 4) iterations are necessary; thereafter, the choice of the nodal plane for each event stabilizes. As the instability factor depends on the coefficient of friction, we also randomly select a coefficient of friction from a uniform distribution between 0.3 and 0.95 for all planes in each realization. We then calculate the medians and standard deviations of $A\phi$ and stress axis orientations across the suite of 5,000 realizations and focus our discussion on these quantities. Uncertainties are given as one standard deviation. Fig. 2a summarizes the results of the 75,000 province-wide realizations, and Fig. 2b summarizes the results of the 310,000 seismic-zone-scale realizations.

Sub-province scale inversions. Figure 2b presents results at scales finer than entire stress provinces, what we term seismic zones. Each province is subdivided into a number of zones in which the style of faulting and principal stress directions appear internally consistent. We require 25 or more mechanisms in each zone and, for clarity, limit lateral dimensions to ~100 km.

Spatially weighted inversions. Figure 2c presents results of spatially weighted stress inversions. Each stress province is divided into a regular Cartesian grid. (Our convention in the text that follows is to refer to this grid in terms of the square `cells' that it comprises and the points, or `nodes', at their centres.) At each node, the nearest 25 mechanisms are selected and inverted following the same methodology as above, but they are weighted inversely by distance from the node. If there are any mechanisms within the cell, they are assigned a weight equal to half the distance between nodes; if a cell subsumes 25 or more mechanisms, all mechanisms within that cell are used and are weighted equally. The node spacing varies from province to province. The minimum node spacing is 33 × 33 km. If such a spacing would require more than $n/2$ nodes within the province, where n is the total number of mechanisms in the province, we increase the spacing such that there are only $n/2$ nodes. For example, New Madrid and central/southern Oklahoma have 33 × 33 km spacing, whereas the province that comprises the northern Plains, Wyoming Craton and Colorado Plateau ($n = 125$) has 224-km node spacing. For computational reasons, we perform only 50 realizations of each inversion. The results are, as elsewhere, the mean across this ensemble of inversions.

Uncertainty of individual mechanisms. The results discussed in the main text are from inversions of many mechanisms, so the uncertainty of any individual mechanism is not a valid proxy for the uncertainty of the inversions that form the basis of our interpretations. Nevertheless, we discuss here the relative uncertainties of the data sources most important to our principal results to determine whether differing weights should be applied. Our primary novel findings are in the CEUS, so we focus our discussion there.

Of the 1,966 mechanisms in the CEUS, a plurality—809—are regional moment tensors derived from surface-waveform fitting[40,41]. These moment tensors are derived by an exhaustive grid search over strike, dip and rake (in 5° increments) and depth. The best-fitting combination, defined as the greatest variance reduction of waveforms, is chosen, but formal uncertainties are not calculated for individual moment tensors. An earlier study[41] presented two independent assessments of the uncertainties associated with this method. First, waveforms from five different frequency bands were used to calculate the moment tensor of an individual event, and three-dimensional angular misfits among the reported slip vectors had a standard deviation of less than 5°. Second, moment tensors for the same set of 181 events were calculated using the same procedure but two completely different catalogues of waveforms and by different groups. Differences between the two sets of solutions are described by Poisson distribution with $\lambda \approx 10°$, meaning that 95% of the solutions were within 15° of one another. Therefore, the 15° of noise that we add to each mechanism during each inversion approximates uncertainty.

The second-largest data source in the CEUS comprises 393 mechanisms from the Mineral, VA, earthquake sequence, derived from P and SH polarities and P, SH and SV amplitudes[42]. These local, high-frequency solutions are nearly identical to another study's[40] regional moment tensors for events for which the latter are available, suggesting that the two data sets are equally reliable. Regardless, our primary results do not depend strongly on the Mineral, VA, area, since we find a similar stress field to that all along the eastern margin of North America.

Of the 344 mechanisms in the New Madrid seismic zone, 273 are based on local P and SH polarities[43]. A previous study[43] performed a grid search over strike, dip and rake for combinations that produce zero polarity errors. To assess uncertainty in strike, dip and rake, the authors calculate the maximum difference between the strike, dip and rake of the median solution and those of all possible solutions, and they reject events with greater than 20° range of possible strike, dip or rake, considering these solutions poorly constrained. This assessment of uncertainty may be conservative, however. For example, take an event with median solution strike/dip/rake of 175/25/−55 and one possible solution of 200/25/−15. The parameter uncertainties are 25/0/40, and the authors of ref. [43] assign an uncertainty of 40° to this event; they would not consider this a reliable focal mechanism. Nevertheless, there is only 18° of difference in the slip vectors. Therefore, the mechanisms reported by these authors are generally constrained to better than 20°. Moreover, we find that excluding the mechanisms of ref. [43] augments the anomalies near New Madrid, increasing $A\phi$ from 1.93 ± 0.02 to 1.95 ± 0.08 and rotating σ_{Hmax} from N83 E ± 1° to N92 E ± 2°.

Our results in central/southern Oklahoma are based almost entirely on regional moment tensors[40], and an earlier study[44] finds a similar strike-slip regime throughout the state. Moreover, another study[15] also shows that this strike-slip regime is distinct from extension in the southern Great Plains to the south, the Rocky Mountain Piedmont to the west and the northern Great Plains to the north.

The final anomaly discussed in the main text is oblique-normal faulting in Eastern Tennessee, and this province has the fewest mechanisms, 59. Of these, 26 are older solutions[45] based on P-wave first motions from local arrivals alone. Excluding these accentuates the anomaly, decreasing $A\phi$ from 0.84 ± 0.07 to 0.73 ± 0.08. Another 25 mechanisms use P and SH polarity[36] and a grid search to define the ensemble of plausible strike/dip/rake. Although uncertainties are not given, distributions of most of these appear (see stereonets in ref. [36]) to be <10°. In addition, one event was modelled in two different studies[36,40], and the solutions agreed to ~10°.

We conclude that the 15° of noise added during inversions approximates the uncertainty in each mechanism. The data sets with the most influence on the anomalies in Oklahoma, New Madrid and Eastern Tennessee have comparable uncertainties, and removing less reliable data sets in New Madrid and Eastern Tennessee would accentuate recovered anomalies.

Sensitivity to friction and pore pressure. The orientation of the shear traction that a certain stress tensor resolves on a certain plane does not depend on the coefficient of friction. Nevertheless, there is a minor effect of friction in our inversions because we do not presume which of the nodal planes is the focal plane and which is the auxiliary. Instead, we calculate the instability factor of the two planes—which depends on friction—and select the more unstable (as proposed by ref. [39]). The resulting $A\phi$ and σ_{Hmax} are statistically friction-independent, however (Supplementary Fig. 4).

For example, inversions of focal mechanisms in New Madrid with a coefficient of friction $\mu = 0.2$ give $A\phi = 1.90 \pm 0.05$ and σ_{Hmax} N83 E ± 1°. With $\mu = 0.9$, these values are 1.93 ± 0.01 and N82 E ± 1°. The anomalies that we observe in Eastern Tennessee and central/southern Oklahoma are also robust with respect to friction, with $A\phi = 0.88 \pm 0.05$ and 1.4 ± 0.01, respectively, for $\mu = 0.2$. We therefore conclude

that, even if low-friction faults localize seismicity in these three zones, frictional weakness cannot directly account for the anomalies that we observe.

Pore-fluid pressure does not affect the orientation of the shear traction either, but it can influence focal mechanism inversions by affecting the diversity of faults that are potentially active and by altering the effectiveness of using the instability factor in selecting the correct nodal plane. An earlier study[46] investigated the pressure dependence of the retrieved stress ratio R

$$R = \frac{\sigma_1 - \sigma_2}{\sigma_1 - \sigma_3}$$

for various `true' R and faulting styles. For all faulting styles, pore pressure and retrieved R are negatively correlated when R is less than ~0.6: if the maximum and intermediate stress are similar in magnitude, then inversions in regions with low pore pressure will estimate a larger difference than is real, and inversions in regions with high pore pressure will estimate an even smaller difference.

Together, the style of faulting and R define $A\phi$ (Supplementary Table 1). Pore-fluid pressure influences R when R is less than ~0.6 and thus $A\phi$ in the ranges of 0.4–1.6 and 2.4–3. In a normal-faulting regime ($0.4 < A\phi < 1$), σ_1 is vertical, and high pore-fluid pressure biases inversions toward higher values of the intermediate stress σ_{Hmax} and therefore $A\phi$. If high pore-fluid pressures are invoked to explain seismicity rates in Eastern Tennessee, then the true $A\phi$ is even lower and the zone is even more anomalous. In strike-slip regimes ($1 < A\phi < 1.6$), σ_2 is vertical, and high pore pressures bias inversions toward a smaller difference between σ_{Hmax} and $\sigma_{vertical}$ (that is, lower values of $A\phi$). If high pore-fluid pressures are invoked to explain comparatively high rates of natural seismicity in central/southern Oklahoma, then $A\phi$ is higher and even more anomalous with respect to the surrounding Great Plains. In New Madrid, $A\phi$ is ~2.0, ($R \sim 0$), so fluid pressure cannot account for the anomalous stress regime.

Short-wavelength stress variations. Large earthquakes perturb the stress field near the fault. The 2002 M7.9 Denali earthquake (combined dextral and reverse slip) ruptured some 300 km with maximum and average displacements of 8 and 4 m (refs [47,48]). Therefore, it is similar in faulting style to and larger in magnitude, displacement and length than the 1811–1812 New Madrid mainshocks. Observations of perturbations to the stress field after the Denali earthquake (within a few years) are therefore presumably a generous proxy for the potential effects of the New Madrid events (200 years later).

Stress inversions of Denali aftershocks suggest that the anomalies in $A\phi$ and σ_{Hmax} in New Madrid are not simply postseismic artefacts. First, aftershock stress inversions differ significantly from pre-mainshock inversions only within ~10 km of the fault patch[24]. Moreover, the only along-strike-consistent difference is a modest clockwise rotation of σ_{Hmax} (by 5°, 10°, 30° and 20°—all ±~15°—in four strike-parallel segments). Changes to $A\phi$ are small and of mixed polarity, with a slight increase in $A\phi$ in the reverse-oblique portion and slight decreases in the purely dextral segments[24]; as a whole, changes to $A\phi$ along the fault are inisignificant. By analogy, rotation of σ_{Hmax} in parts of the New Madrid seismic zone could be the result of postseismic processes, but this anomaly should not be pervasive throughout the zone, and no overall anomalies in $A\phi$ are likely to result from the 1811–1812 mainshocks.

Charleston, SC, and Mineral, VA (locations in Fig. 1a), provide additional examples of stress changes in aftershock sequences. Within ~5 km of the mainshock epicentres, strong spatial dependence of S_H but consistent faulting style (Supplementary Fig. 5) resemble the patterns observed in Denali aftershocks. Specifically, thrust faulting abounds in both zones, but S_H is roughly radial about the mainshocks. This pattern resembles the Coulomb stress-transfer field expected for the proposed mechanism in Charleston[47,49] and the moment tensor of the Mineral event[40].

With only 52 mechanisms surrounding the Charleston mainshock, we cannot quantify spatial σ_{Hmax} variations, but another study[42] presents nearly 400 focal mechanisms near Mineral, and we use these to perform inversions in small zones (about 0.25–25 km^2; containing at least 25 mechanisms) surrounding the mainshock (Supplementary Fig. 5C). Results are consistent with our interpretation based on S_H: beyond ~5 km from the epicentre, σ_{Hmax} trends approximately ESE–WNW but rotates to approximately SSE–WNW to the north and northwest and NNE–SSW to the south and west of the epicentre.

By contrast, a similar analysis in New Madrid does not reveal substantial spatial dependence (Supplementary Fig. 5B,D). First, reverse-oblique motion occurs throughout the seismic zone rather than being confined to areas within a few kilometres of certain faults, inconsistent with alteration of $A\phi$ by previous mainshocks (as is the analogy with Denali, where $A\phi$ is not systematically altered). Second, stress inversions in latitudinal bins of ~30 mechanisms reveal that, although there is modest variation at length scales of tens of kilometres, both $A\phi$ and σ_{Hmax} are consistently different from the rest of the Midwest. Along the southern arm of seismicity (the Cottonwood Grove or Axial Fault), σ_{Hmax} is N86 E and $A\phi$ is 1.80, whereas the rest of the seismic zone displays σ_{Hmax} of approximately N80–85 E and $A\phi$ of 2.10–2.23. The clockwise rotation of σ_{Hmax} along the Cottonwood Grove fault is similar to what would be expected surrounding a dextral strike-slip fault[39], and by analogy with the Denali earthquake, one might also expect slightly suppressed $A\phi$ near the fault. We suggest that the differences between the Cottonwood Grove and other faults in the zone illustrate the small influence of postseismic processes. Nevertheless, σ_{Hmax} and $A\phi$ are statistically different in all parts of the zone from its surroundings, so the anomalous state of stress in New Madrid is unlikely to be the result of the influence from prior earthquakes.

Similarly, we find only minor spatial dependence in the state of stress in central/southern Oklahoma and Eastern Tennessee. In central and northern Oklahoma, another study[44] also performs stress inversions in small (~50 × 50 km) zones, also finding essentially constant σ_{Hmax} and a systematic transition from normal and oblique-normal faulting ($A\phi \lesssim 1$) to strike-slip faulting ($A\phi$ up to 1.38) from northern to central Oklahoma. Thus, we argue that any internal variations in the states of stress in New Madrid, Eastern Tennessee and central/southern Oklahoma are small compared to their respective differences with surrounding regions. Instead, each seismic zone is consistently different from its surroundings, casting doubt on the role of short-length-scale perturbations such as from postseismic processes or stress transfer.

Code availability. Stress inversion codes (written for MATLAB) are freely available from the corresponding author.

Data availability. The focal mechanism database is presented in the Supplementary Information; in situ indicators are presented by ref. [9]. The results presented in Fig. 2c are displayed as a comma-delimited [Lon,Lat,σ_{Hmax},$A\phi$,uncertainties] file in the Supplementary Information.

References

37. Wallace, R. E. Geometry of shearing stresses and relation to faulting. *J. Geol.* **59**, 118–130 (1951).
38. Bott, M. H. P. The mechanics of oblique-slip faulting. *Geol. Mag.* **96**, 109–117 (1959).
39. Varryčuk, V. Iterative joint inversion for stress and fault orientations from focal mechanisms. *Geophys. J. Int.* **199**, 69–77 (2014).
40. Herrmann, R. B. *Moment Tensors for North America* (St Louis Univ. accessed 1 January 2018); http://www.eas.slu.edu/eqc/eqc_mt/MECH.NA/MECHFIG/mech.html
41. Herrmann, R. B., Malagnini, L. & Munafó, I. Regional moment tensors of the 2009 L'Aquila earthquake sequence. *Bull. Seismol. Soc. Am.* **101**, 975–993 (2011).
42. Wu, Q., Chapman, M. C. & Beale, J. N. The aftershock sequence of the 2011 Mineral, Virginia earthquake: temporal and spatial distribution, focal mechanisms, regional stress, and the role of Coulomb stress transfer. *Bull. Seismol. Soc. Am.* **105**, 2521–2527 (2015).
43. Johnson, G. A., Horton, S. P., Withers, M. & Cox, R. Earthquake focal mechanisms in the New Madrid seismic zone. *Seismol. Res. Lett.* **85**, 257–267 (2014).
44. Walsh, F. R. III & Zoback, M. D. Probabilistic assessment of potential fault slip related to injection-induced earthquakes: application to north-central Oklahoma, USA. *Geology* **44**, 991–994 (2016).
45. Chapman, M. C. et al. A statistical analysis of earthquake focal mechanisms and epicenter locations in the Eastern Tennessee Seismic Zone. *Bull. Seismol. Soc. Am.* **87**, 1522–1536 (1997).
46. Martinez-Garzón, P. J. et al. Sensitivity of stress inversion of focal mechanisms to pore pressure changes. *Geophys. Res. Lett.* **43**, 8441–8450 (2016).
47. Haeussler, P. J. et al. Surface rupture and slip distribution of the Denali and Totschunda faults in the 3 Novermber 2002 M7.9 earthquake, Alaska. *Bull. Seismol. Soc. Am.* **94**, S23–S52 (2004).
48. Hreinsd¢ttir, S. et al. Coseismic deformation of the 2002 Denali fault earthquake: insights from GPS measurements. *J. Geophys. Res.* **111**, B03308 (2006).
49. Chapman, M. C. et al. Modern seismicity and the fault responsible for the 1886 Charleston, South Carolina, earthquake. *Bull. Seismol. Soc. Am.* **106**, 364–372 (2016).